# CFD Analysis of a Spent Nuclear Fuel Dry Storage Cask Using an LTNE Porous Media Model

Tae Gang Lee <sup>a</sup>, Jae Jun Jeong <sup>a\*</sup>, Tae Hyung Na<sup>b</sup>.

<sup>a</sup>School of Mechanical Engineering, Pusan National University (PNU)

<sup>b</sup>Central Research Institute, Korea Hydro & Nuclear Power Co., Ltd

\*Corresponding author: jjjeong@pusan.ac.kr

\*Keywords: Spent nuclear fuel, dry storage, thermal analysis, LTNE porous.

#### 1. Introduction

The storage of spent nuclear fuel (SNF), particularly from pressurized water reactors (PWRs), has become an increasingly critical issue in recent years. In Korea, the saturation of PWR spent fuel pools has emerged as a major concern, and the operator, KHNP, is seeking to address this problem through the construction of interim dry storage facilities [1].

Thermal analysis is essential for the design and safety assessment of such facilities, since the temperature of the SNF directly determines fuel integrity and material integrity. The temperatures of internal and external components affect material properties, oxidation behavior, and long-term durability; thus, accurate thermal predictions are required [2 - 5].

Earlier studies often adopted highly conservative assumptions—such as limited heat transfer—to ensure cladding integrity [6]. However, more realistic analyses are now required, including predictions of material temperature histories and system responses under long-term storage conditions. Various analysis approaches, such as simplified 1D codes, subchannel codes, the conventional Local Thermal Equilibrium (LTE) porous model, and full rod-by-rod CFD models, have been considered [6 - 9]. Each approach, however, faces limitations in either high computational cost or the ability to capture realistic heat transfer mechanisms.

To address these challenges, this study applies the Local Thermal Non-Equilibrium (LTNE) porous media model[10-12]. Unlike LTE models, LTNE separately solves the solid and fluid energy equations, enabling prediction of temperature differences between the solid structure and the interstitial fluid. This approach allows convective heat transfer to be treated more realistically and offers a practical compromise between accuracy and computational cost.

To evaluate the applicability of the LTNE porous media model for the thermal analysis of SNF dry storage systems, the TN-24P storage cask test [6] was selected as a benchmark. The TN-24P is a forged-steel cylindrical cask approximately 5 m in height and 2.3 m in diameter, accommodating twenty-four 15 × 15 PWR fuel assemblies stored in an aluminum fuel basket, as illustrated in Fig. 1 and Fig. 2. The experiments were conducted under six conditions, combining vertical and

horizontal orientations with different backfill gases (helium, nitrogen, and vacuum).

In this study, the vertical, nitrogen-filled configuration was chosen as the benchmark case, since it represents the most common storage orientation and exhibits stronger natural convection than the helium-filled case. The primary objective of this work is therefore to assess the applicability of the LTNE porous media model as a practical and accurate tool for cask thermal analysis.

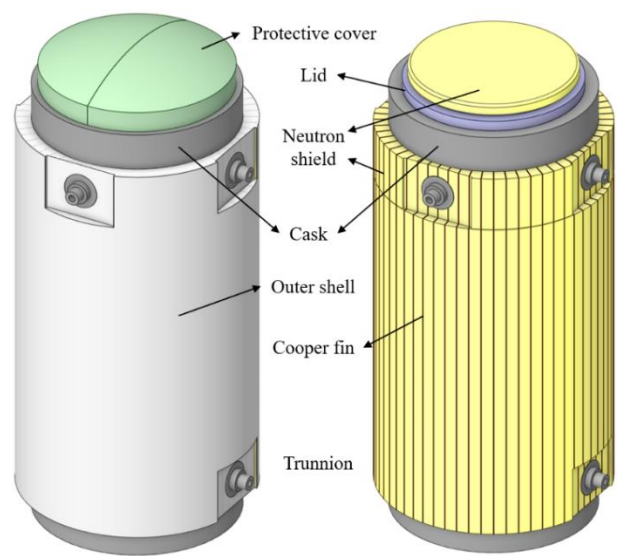


Fig. 1. Schematic of the TN-24P cask outside.

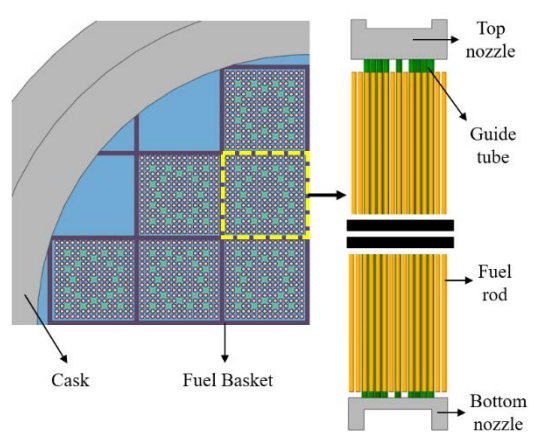


Fig. 2. Schematic of the TN-24P cask inside and 15X15 PWR fuel.

#### 2. Methods

Dry storage casks such as the TN-24P typically accommodate thousands of fuel rods. Representing every rod individually in a numerical calculation would lead to prohibitively high computational costs. A porous media model inevitably loses local information of individual rods, but in exchange it provides a dramatic gain in computational efficiency, making full-cask calculations feasible. In this study, each 15×15 PWR fuel assembly (FA) is modeled as an equivalent porous medium using the LTNE approach.

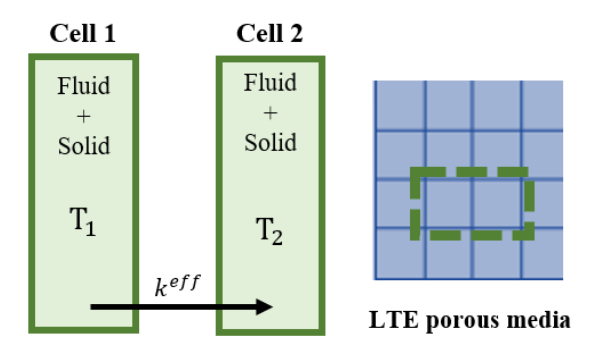


Fig. 3. Heat transfer in LTE porous media.

As illustrated in Fig. 3, the conventional porous approach based on LTE assumes a single temperature for both solid and fluid phases, with intercell heat transfer expressed only by an effective conductivity, keff. In reality, however, temperature differences exist between the fuel rods and the backfill gas, which strongly influence convective heat transfer. As a result, the effect of convection is obscured within keff; in other words, conduction, convection, and radiation are all lumped into a single effective property. Consequently, the LTE assumption cannot adequately capture the actual heat transfer mechanisms [12].

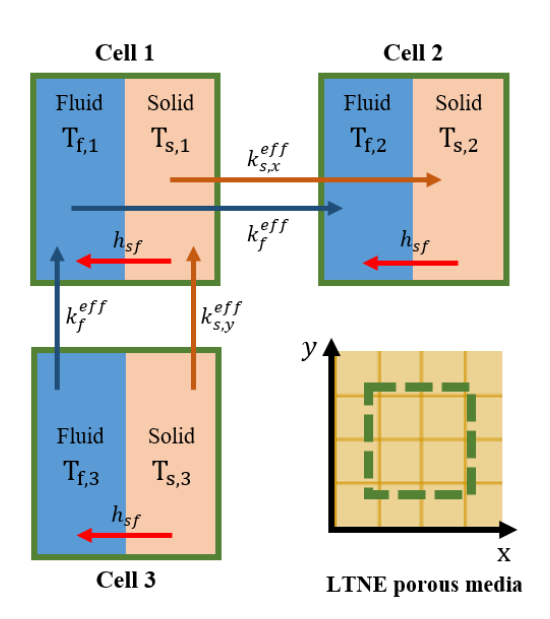


Fig. 4. Heat transfer in LTNE porous media.

In contrast, the LTNE model [10, 11, 12], illustrated in Fig. 4, distinguishes between solid and fluid phases and solves separate energy equations for each. The interfacial heat transfer coefficient (hsf) governs energy exchange between phases within a cell, while conduction between neighboring cells is described separately by the effective solid conductivity (ks eff) and effective fluid conductivity (k<sub>f</sub><sup>eff</sup>). Radiation effects are still incorporated indirectly into the effective conductivity, but convection is explicitly represented through h<sub>sf</sub>. This separation enables a more realistic representation of the coupled conduction-convection processes inside the porous medium.

The steady-state governing equations for LTNE porous media can be expressed as follows [11]:

For fluid phase:

$$\nabla \cdot (\varepsilon \rho_f c_{pf} \overrightarrow{U} T_f) = \nabla \cdot (\varepsilon k_f^{eff} \nabla T_f) + h_{sf} a_{ef} (T_s - T_f) + Q_f, (1)$$
For solid phase:

For solid phase: 
$$\nabla \cdot \left[ (1 - \varepsilon) k_s^{eff} \nabla T_s \right] + h_{sf} a_{eff} (T_f - T_s) + Q_s = 0, \qquad (2)$$

where  $\varepsilon$  is the porosity,  $\alpha_{sf}$  is the interfacial area density, h<sub>sf</sub> is the interfacial heat transfer coefficient, and Q<sub>f</sub> and Qs are volumetric heat sources. To model an FA as a porous medium, it is essential to determine k<sub>s</sub> eff, k<sub>fe</sub> ff, and h<sub>sf</sub> in a physically consistent manner. For example, considering the anisotropic geometry of the FA, the effective conductivity of the solid phase should be defined directionally to capture bundle-scale heat transfer characteristics.

To determine these parameters, detailed CFD simulations of a representative FA were conducted. From these simulations, flow resistance characteristics and heat transfer coefficients were obtained, and the LTNE porous parameters (k<sub>s</sub> eff, k<sub>f</sub> eff, h<sub>sf</sub>) were derived. The performance of the porous model was then examined by comparing its predictions with the detailed FA simulations, using the peak cladding temperature (PCT) as the primary metric.

Finally, the porous model was applied to the TN-24P cask analysis. One limitation of the LTNE implementation in ANSYS Fluent is that it cannot be directly combined with the radiation model [11]. To address this, radiation heat transfer was incorporated by assigning equivalent heat generation conditions to the surface by user-defined functions (UDFs) [13]. This approach enabled conduction, convection, and radiation to be consistently included in the analysis. The TN-24P simulation results were subsequently compared with experimental data for validation.

## 3. Development of LTNE Porous Model

### 3.1 Detailed Fuel Assembly Analysis

As discussed in Section 2, it is essential to identify the thermal-hydraulic characteristics inside the FA in order to reasonably determine the porous parameters. Therefore, a detailed thermal—hydraulic calculation was performed for a single 15×15 PWR FA stored in the TN-24P cask. The top and bottom nozzles were excluded from the geometry, and one-quarter symmetry was applied to reduce computational cost. The computational mesh, shown in Fig. 5, consisted of structured grids with approximately 16.8 million cells.

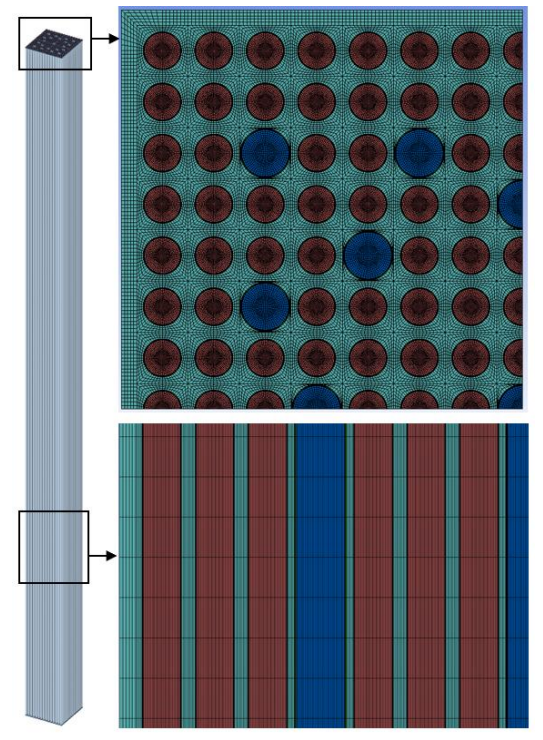


Fig. 5. The mesh of the detailed FA analysis input.

The internal flow was assumed to be laminar. Buoyancy effects were modeled using the Boussinesq approximation, and density variations were calculated with the ideal gas law. Radiation was modeled using the Discrete Ordinates (DO) method, which is suitable for the complex FA geometry [11, 12]. The calculations were performed on an AMD Ryzen Threadripper 3.79 GHz processor with 36 cores and required more than 110 hours to converge.

Boundary conditions were determined based on TN-24P experimental data and COBRA-SFS predictions [6], as summarized in Table 1. Three calculation cases were conducted. From each case, the peak cladding temperature (PCT) and the average Rayleigh number (Ra) were obtained, as listed in Table 1. The average Rayleigh number [13] was defined as

$$Ra = \frac{g\beta q''H^4}{\bar{k}_f \bar{v} \; \bar{\alpha}} \,, \tag{3}$$

where g is gravitational acceleration,  $\beta$  is the thermal expansion coefficient (evaluated through the Boussinesq approximation), q" is the surface heat flux of fuel rods, H is the length of FA,  $\overline{k}_f$  is the average thermal conductivity of the fluid,  $\overline{\nu}$  is the average kinematic

viscosity, and  $\bar{\alpha}$  is the average thermal diffusivity. Based on these results, the flow was clearly categorized as laminar (Ra < 1000~2000), which justifies the use of laminar porous correlations in the following parameter derivations.

Table I: Boundary conditions for detailed FA analysis and the results.

	Case 1	Case 2	Case 3
Decay heat per FA			
[W]	750	1000	1250
(Heat Flux	(25.34)	(33.78)	(42.23)
[W/m2])			,
Basket wall	100	150	200
temperature [°C]	100	130	200
Inlet velocity [°C]	0.1	0.1	0.1
PCT [°C]	185.4	219.3	250.4
Ra [-]	628	741	828

#### 3.2 Effective Thermal Conductivity

Because radiation cannot be directly solved within the porous domain, its effect must be incorporated into the effective thermal conductivity. For the fluid phase, heat transfer is assumed isotropic and radiation is negligible, so the conductivity of nitrogen,  $k_f^{\rm eff}$ , was directly adopted. For the solid phase, however, the FA geometry leads to strongly anisotropic conduction characteristics.

Along the axial (y) direction, conduction dominates heat transfer; therefore, the effective conductivity,  $k_{s,y}^{eff}$ , was determined as a weighted average of the constituent materials. In the radial (x, z) plane, radiation must be considered in addition to conduction. To account for this, the methodology of Bahney and Lotz [15] was followed. Using the detailed FA CFD input, a two-dimensional radial model was constructed, and cladding temperature responses to different power and boundary conditions were evaluated. From these calculations, a third-order polynomial correlation was obtained for the effective radial conductivity as a function of wall temperature and power level.

$$k_{s,x/z}^{\text{eff}} = 8.58 \times 10^{-10} T^3 - 1.36 \times 10^{-7} T^3 - 3.6 \times 10^{-5} T + 0.038$$
 (4)

## 3.2 Flow Resistance

Flow resistance inside the porous medium was modeled using the Darcy–Forchheimer relation [16]:

$$-\nabla p = \mu \frac{1}{K} \vec{U} + C_2 \frac{1}{2} \rho \vec{U} \left| \vec{U} \right|, \tag{5}$$

where K is the permeability and C<sub>2</sub> is the inertial resistance coefficient. To determine these values, pressure drop calculations were conducted using the fluid region of the FA model. By varying the inlet velocity, the relation between pressure gradient and

velocity was obtained, from which K and C<sub>2</sub> were derived. The final values are summarized in Table 2.

Table II: Permeability, K, and inertial resistance coefficient, C<sub>2</sub>, calculated from the detailed FA analysis input.

Direction	K [m <sup>2</sup> ]	$C_2 [m^{-1}]$
X	6.34e-7	197.88
у	1.06e-6	7.62
Z	6.34e-7	197.88

## 3.4 Interfacial Heat Transfer Coefficient

As the FA flow was evaluated to be laminar, correlations based on the Rayleigh–Darcy number, Ra\*, were employed to estimate the interfacial heat transfer coefficient. Among the available options, the Cheng–Minkowycz correlation [17] has been widely and reliably applied for porous natural convection:

$$Nu = 0.444(Ra^*)^{0.5}, (6)$$

where the Rayleigh-Darcy number [18] is defined as:

$$Ra^* = \frac{g\beta(T_s - T_f)KD_h}{\alpha \nu},$$
(7)

where  $T_s$  and  $T_f$  are the solid and fluid temperatures in the LTNE porous media, respectively; K is the permeability; and  $D_h$  is the hydraulic diameter. In porous media, the hydraulic diameter is given as

$$D_h = \frac{4\varepsilon}{\alpha_{sf}},\tag{8}$$

where the interfacial area density  $\alpha_{sf}$  = interface area / fluid volume, and the porosity  $\epsilon$  = fluid volume / total volume.

## 3.5 Performance Assessment

The performance of the developed LTNE porous model was examined by comparing its predictions with the detailed FA calculations. Table 3 summarizes the results, where the PCT was used as the primary comparison metric. The porous model slightly overpredicted the PCT as the heat generation increased, which can be attributed to the conservative interfacial heat transfer correlations applied because of laminar flow. Nevertheless, the deviation remained below 3%, indicating that the developed LTNE porous model can reasonably reproduce the thermal behavior of the FA. Therefore, it was concluded that the developed model is suitable for application to the TN-24P cask analysis.

Table III: Comparison of calculated PCT.

	Case 1	Case 2	Case 3
Detailed FA [°C]	185.4	219.3	250.4

LTNE [°C]	187.6	227.8	262.5
Δ	+ 1.8	+ 8.5	+ 12.1
Difference [%]	0.51	0.04	2.32

## 4. TN-24P Cask Analysis

## 4.1 CFD input for TN-24P

The LTNE porous media model developed in this study was applied to the TN-24P cask analysis input. To reduce computational cost and focus on the primary thermal–hydraulic behavior, several external components of the experimental cask—such as the outer shell, neutron shield, copper fins, protective cover, and trunnions—were excluded from the computational domain. Furthermore, one-quarter symmetry of the geometry was employed.

The finalized mesh, determined through the independence study, contained approximately 6.9 million cells, more than 97% of which were structured. In regions with high curvature or small lattice, trigonal cells were unavoidably used. The mesh configuration is shown in Fig. 6.

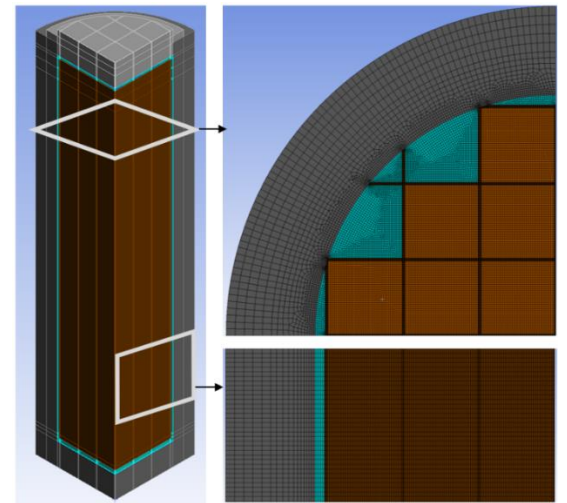


Fig. 6. The mesh of the TN-24P analysis.

The physical models were set up in a similar manner consistent with the detailed FA input. The internal flow was assumed laminar, while natural convection was modeled using the Boussinesq approximation. Density variation was modeled using the ideal gas law, which drives natural convection [11, 12].

The major difference lay in the treatment of radiation. As noted in Section 2, the LTNE model in FLUENT cannot be directly coupled with the built-in radiation models, such as the DO model. Therefore, user-defined functions (UDFs) were developed to represent radiative heat transfer. The first implementation targeted surface-to-surface radiation inside the cask. Radiative source terms were imposed on the cask surfaces using the heat

generation boundary condition. View factors were evaluated by the Monte Carlo method, and surface-averaged temperatures were updated at each iteration. The corresponding radiative heat fluxes were then obtained using the Gauss–Seidel method and applied through the UDF [13]. In addition, radiation across the porous solid–basket interface was also considered. In the LTNE framework of FLUENT, heat transfer does not occur at this interface unless explicitly modeled. To address this limitation, another UDF was applied to account for radiative exchange between adjacent cells across the interface. The net radiative flux was expressed

$$q_{rad}^{"} = \frac{1}{\frac{1}{\lambda_{porous,s}} + \frac{1}{\lambda_{basket}} - 1} \sigma \left( T_{porous,s}^4 - T_{basket}^4 \right) . \tag{9}$$

where  $\lambda_{porous,s}$  and  $\lambda_{basket}$  are the surface emissivities of the porous solid and basket, respectively.

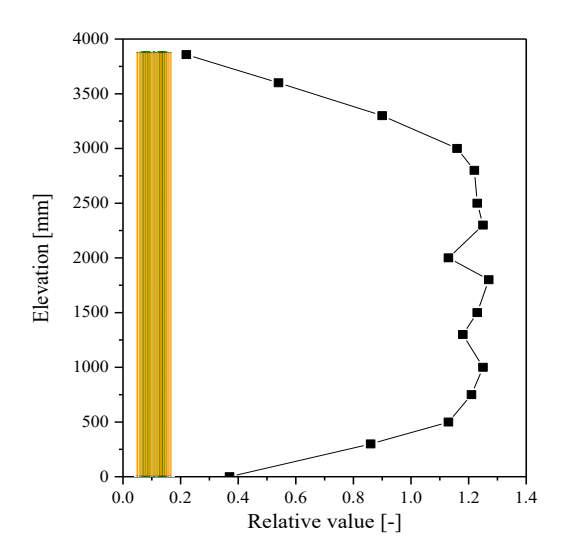


Fig. 7. Predicted axial decay heat profile [6].

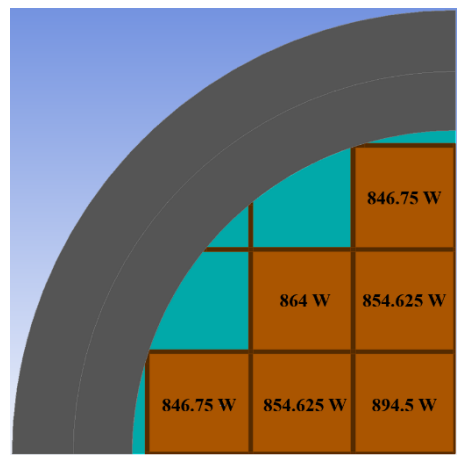


Fig. 8. Heat source assigned to each fuel assembly represented by porous media [6].

Boundary conditions on the cask outer wall were set as an isothermal wall temperature condition. Experimental measurements showed most of the surface, covered by the neutron shield, remained within 65–75 °C. Considering the high thermal conductivity of forged steel, a uniform wall temperature of 69 °C was applied [6].

The internal heat generation was prescribed according to the axial decay heat profile (Fig. 7) and the total decay heat of each FA—represented as an equivalent porous medium—was assigned based on the values in Fig. 8 [6]. Other boundary conditions, such as pressure, were applied using experimental measurements.

# 4.2 Analysis results

The computational setup was identical to that of the detailed FA analysis, and the total runtime was approximately 3.4 hours. Due to the poor convergence characteristics inherent to natural convection in an enclosed domain, convergence was assessed by monitoring the peak cladding temperature (PCT). When the difference in PCT between successive iterations was less than 0.01 °C, the solution was considered converged.

The results are summarized in Fig. 9 and Table 4. The predicted PCT was 233 °C, which deviated by about 0.4% from the experimental measurement (232 °C) and by about 5.7% from the COBRA-SFS prediction (247 °C). Overall, the LTNE model–based analysis provided reasonable agreement with both the experimental data and system code calculations. Considering that the design criteria were PCT < 400 °C, there was a significant margin between both the measured and calculated values.

Table IV: Comparison of PCT between experiment, COBRA-SFS, and LTNE mode.

	Experiment	COBRA- SFS	LTNE
PCT [°C]	232	247	233

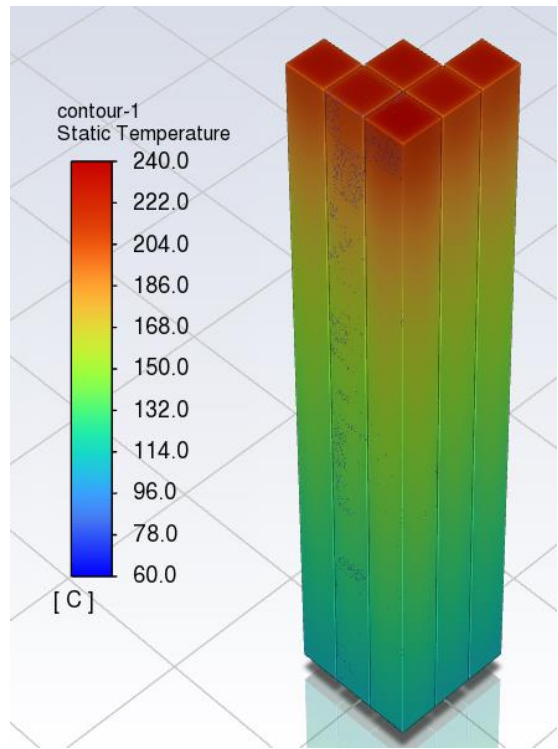


Fig. 9. Temperature contour of the LTNE porous media.

## 5. Conclusions

In this study, the applicability of the LTNE porous media model to the thermal analysis of PWR spent nuclear fuel dry storage systems was evaluated. As a benchmark, the vertical, nitrogen-filled case of the TN-24P dry storage cask test was selected. To develop the porous model, a detailed CFD analysis of a single fuel assembly was performed, from which the porous parameters—effective thermal conductivities, flow resistance coefficients, and interfacial heat transfer coefficient-were derived. The developed model showed deviations of less than 3% in peak cladding temperature (PCT) compared with the detailed FA analysis, demonstrating its capability to reasonably represent the thermal-hydraulic behavior of the fuel assembly. The model was then applied to the TN-24P cask input. The radiation in the cask was implemented via a UDF using the heat generation condition. When compared with experimental data, the predicted PCT deviated by less than 0.4%, which was considered reasonable. These results confirm that the developed LTNE model is sufficiently applicable to the safety analysis of dry storage systems.

Future work will focus on a detailed evaluation of flow and radiation behavior within fuel assemblies to identify and apply the most appropriate interfacial heat transfer and radiation models for input preparation. In addition, other benchmark cases of the TN-24P test will be analyzed to further extend the applicability of the model.

#### REFERENCES

- [1] National Assembly of Korea, High-Level Radioactive Waste Management Act, Republic of Korea, 2025.
- [2] U.S. NRC, Title 10, Code of Federal Regulations, Part 72 – Licensing Requirements for the Independent Storage of Spent Nuclear Fuel, High-Level Radioactive Waste, and Reactor-Related Greater Than Class C Waste, 2024.
- [3] U.S. NRC, NUREG-2152: Spent Fuel Transportation Risk Assessment, 2012.
- [4] U.S. NRC, NUREG-2215: Standard Review Plan for Spent Fuel Dry Storage Systems and Facilities, 2020.
- [5] F. P. Beer, E. R. Johnston, J. T. DeWolf, and D. F. Mazurek, Mechanics of Materials, 7th ed., McGraw-Hill, New York, 2015.
- [6] R. E. Einziger, R. E. Mason, and D. K. Morton, The TN-24P PWR Spent-Fuel Storage Cask: Testing and Analyses, Sandia National Laboratories, Albuquerque, N.M., 1989.
- [7] J.-C. Lee, K.-S. Bang, K.-S. Seo, and H.-D. Kim, "Thermal analysis of a storage cask for 24 spent PWR fuel assemblies," Annals of Nuclear Energy, Vol. 28, pp. 533–546, 2001.
- [8] S. H. Yoo, H. C. Kim, and J. Y. Jeong, "Full-scope simulation of a dry storage cask using computational fluid dynamics," Nuclear Engineering and Design, Vol. 240, pp. 2286–2294, 2010.
- [9] R. A. Brewster, D. R. Oland, and B. P. Boyack, "CFD analyses of the TN-24P PWR spent fuel storage cask," in Proc. ASME PVP Conf., Toronto, Canada, 2012.
- [10] Y. Yun, H. S. Choi, and C. H. Song, "Natural convection heat transfer characteristics in a canister with horizontal installation of dual purpose cask for spent nuclear fuel," Nuclear Engineering and Technology, Vol. 53, No. 10, pp. 3189–3199, 2021.
- [11] ANSYS Inc., ANSYS Fluent User's Guide, Release 2021 R2, 2021.
- [12] ANSYS Inc., ANSYS Fluent Theory Guide, Release 2021 R2, 2021.
- [13] ANSYS Inc., ANSYS Fluent UDF Manual, Release 2021 R2, 2021.
- [14] F. P. Incropera, D. P. DeWitt, T. L. Bergman, and A. S. Lavine, Fundamentals of Heat and Mass Transfer, 8th ed., John Wiley & Sons, Hoboken, NJ, 2017.
- [15] U.S. DOE, Spent Nuclear Fuel Effective Thermal Conductivity Report, TRW Environmental Safety Systems, Inc., Yucca Mountain Project Office, Las Vegas, N.V., July 11, 1996.
- [16] A. Bejan, Convection Heat Transfer, 4th ed., John Wiley & Sons, Hoboken, NJ, 2013.
- [17] P. Cheng and W. Minkowycz, "Free convection about a vertical flat plate embedded in a porous medium with application to heat transfer from a dike," Journal of Geophysical Research, Vol. 82, pp. 2040–2044, 1977.

## Transactions of the Korean Nuclear Society Autumn Meeting Changwon, Korea, October 30-31, 2025

[18] D. A. Nield and A. Bejan, Convection in Porous Media, 3rd ed., Springer, New York, 2006.